Supporting Information

Interactions of IOX1, a histone demethylase inhibitor, with essential metal ions, albumin, and its clay-based nanoformulation

Hilda Kovács,[a] Orsolya Dömötör,[a] Anett Giricz,[a] Nóra Igaz,[b] Krisztina Szőke, [b] Csenge Bocz, [b] Mónika Kiricsi, [b] Adél Szerlauth,[c] Réka Ormos, [c] István Szilágyi, [c] Éva A. Enyedy[a,*]

[a]H. Kovács, O. Dömötör, A. Giricz, É. A. Enyedy, Department of Molecular and Analytical Chemistry University of Szeged, Dóm tér 7-8, H-6720 Szeged, Hungary
e-mail: enyedy@chem.u-szeged.hu

[b]N. Igaz, K. Szőke, C. Bocz, M. Kiricsi, Department of Biochemistry and Molecular Biology University of Szeged, Közép fasor 52, H-6726 Szeged, Hungary

[c]A. Szerlauth, R. Ormos, I. Szilágyi, MTA-SZTE „Momentum" Biocolloids Research Group, Department of Physical Chemistry and Materials Science, University of Szeged, Rerrich Béla tér 1, H-6720 Szeged, Hungary

Table of contents

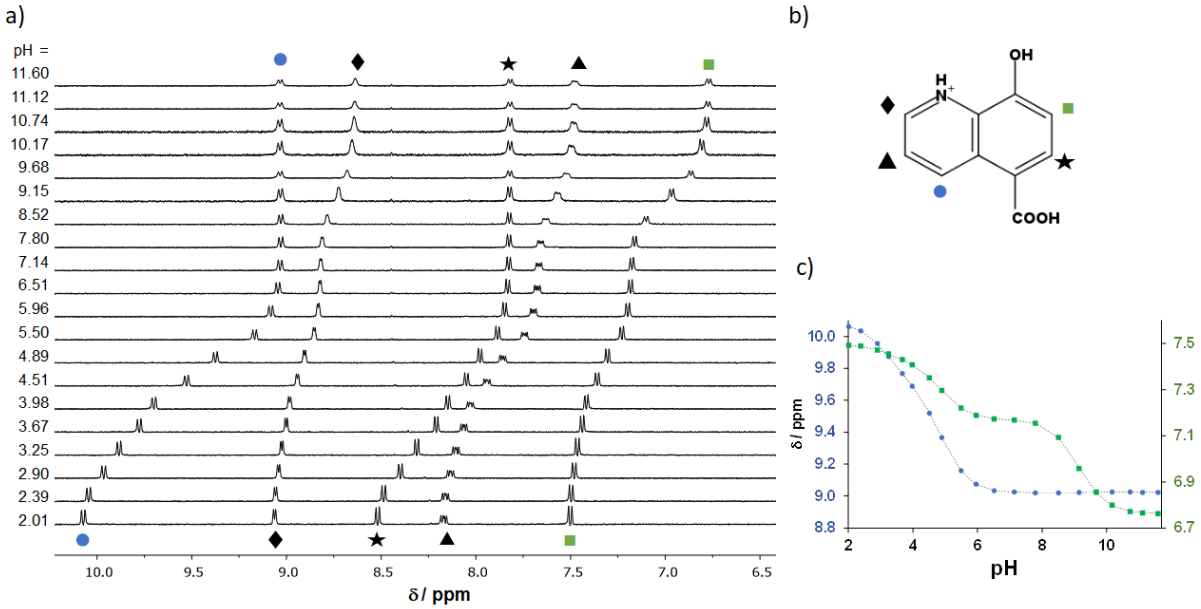

Figure S1. (a) ^{1}H NMR spectra recorded for IOX1 in the pH range 2.0–11.6. (b) Chemical structure of the fully protonated ligand with the notation of the symbols of the CH protons. (c) Chemical shifts of two selected protons (C4H (●) & C7H (■) at various pH values with the fitted curve (dashed lines). {c_{IOX1} = 700 μM; I = 0.2 M (KNO_3); 10% (*v/v*) D_2O/H_2O; T = 25.0 °C}

Table S1. pK_a values of 2-OG and overall stability constants (logβ) of Fe(III) complexes determined by UV-vis spectrophotometric titrations, and logβ of Fe(II) complexes obtained by pH-potentiometry.[a] {T = 25.0 °C; I = 0.1 M (KCl)}

	2-OG		
pK_a	pK_1 = 1.74 ± 0.04		pK_2 = 4.52 ± 0.03
logβ	Fe(III)		Fe(II)
method	*pH-metry*[b]	*UV-vis*[c]	*pH-metry*[d]
[MLH]	–	8.90 ± 0.06	7.06 ± 0.09
[ML]	5.2	5.89 ± 0.09	–
[ML$_2$]	8.2	10.5 ± 0.2	–

[a] Charges of the complexes are omitted for clarity. L^{2-} is doubly negative. [b] Formation constants for Fe(III) complexes taken from Ref. SI1 [c] Data were evaluated at pH < 4. [d] Data were evaluated at pH < 7.

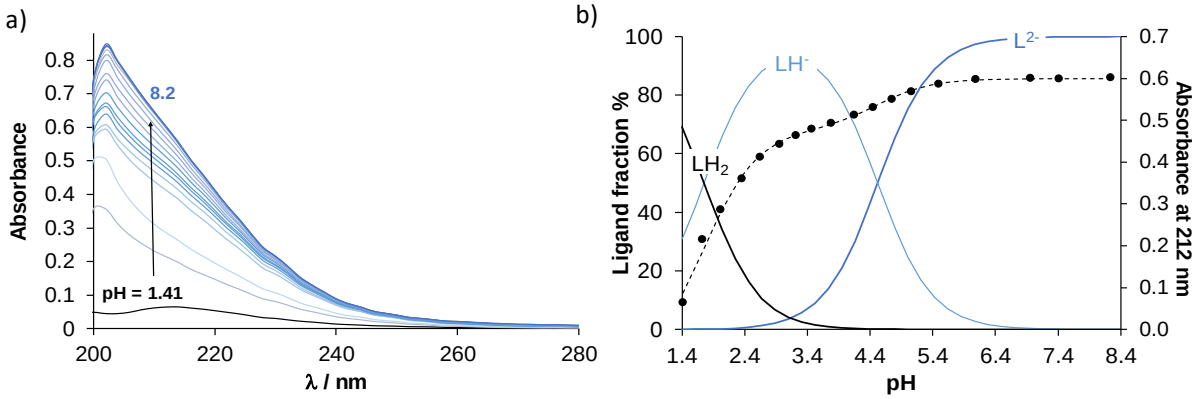

Figure S2. (a) UV-vis absorption spectra recorded for 2-OG in the pH range 1.4 – 8.2 (b) Concentration distribution curves calculated with the pK_a values obtained by UV-vis titrations, and absorbance changes at 212 nm (●) at various pH values with the fitted curve (dashed line). {c_{IOX1} = 300 μM; ℓ = 1 cm; I = 0.1 M (KCl); T = 25.0 °C}

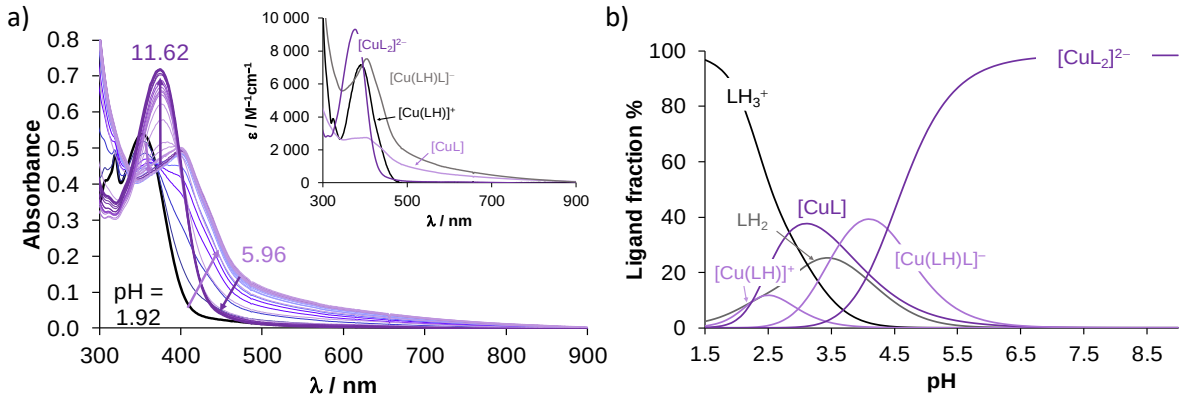

Figure S3. (a) UV-vis absorption spectra recorded for the Cu(II) – IOX1 (1:2) system in the pH range 2.1 – 11.6, the inserted figure shows the calculated UV-vis molar absorption spectra of the various complexes (b) Concentration distribution curves calculated for the same system. {c_{IOX1} = 161 µM; $c_{Cu(II)}$ = 80 µM; ℓ = 1 cm; I = 0.1 M (KCl); T = 25.0 °C}

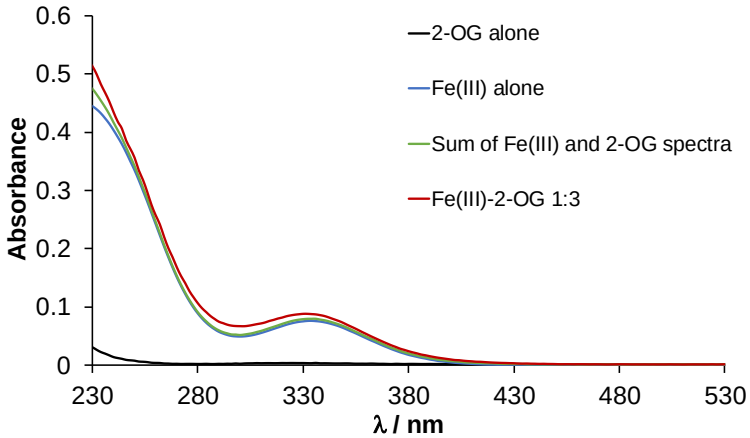

Figure S4. UV-vis absorption spectra recorded for 2-OG alone (black), Fe(III) alone (blue), sum of 2-OG and Fe(III) (green), and Fe(III) – 2-OG 1:3 system (red) at pH 1.40. {$c_{2\text{-OG}}$ = 300 µM; $c_{Fe(III)}$ = 100 µM; ℓ = 1 cm; I = 0.1 M (KCl); T = 25.0 °C}

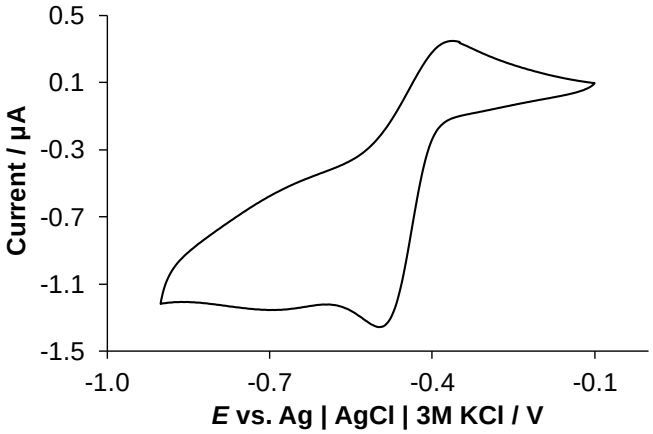

Figure S5. Cyclic voltammogram of the Fe(III) – 2-OG (1:3) system. {$c_{2\text{-OG}}$ = 1.5 mM; $c_{Fe(III)}$ = 0.5 mM; pH = 3.00; 60% (*v*/*v*) DMF/H_2O; scan rate: 10 mV/s; I = 0.1 M (KNO_3); T = 25.0 °C}

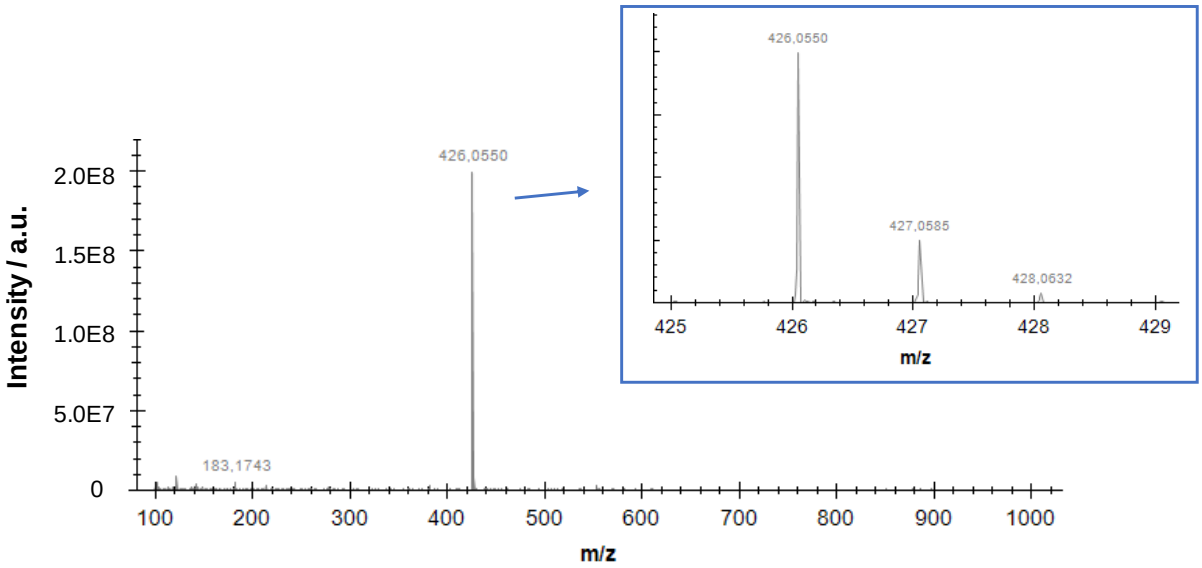

Figure S6. ESI-MS spectrum of [RhCp*(LH)(H_2O)] complex, m/z values for $[RhCp^*(LH)]^+$ ($C_{20}H_{21}NO_3Rh$): calculated: 426.0576, found: 426.0550. {$c_{complex}$ = 200 µM; pH = 7.4 (NH_4HCO_3)}

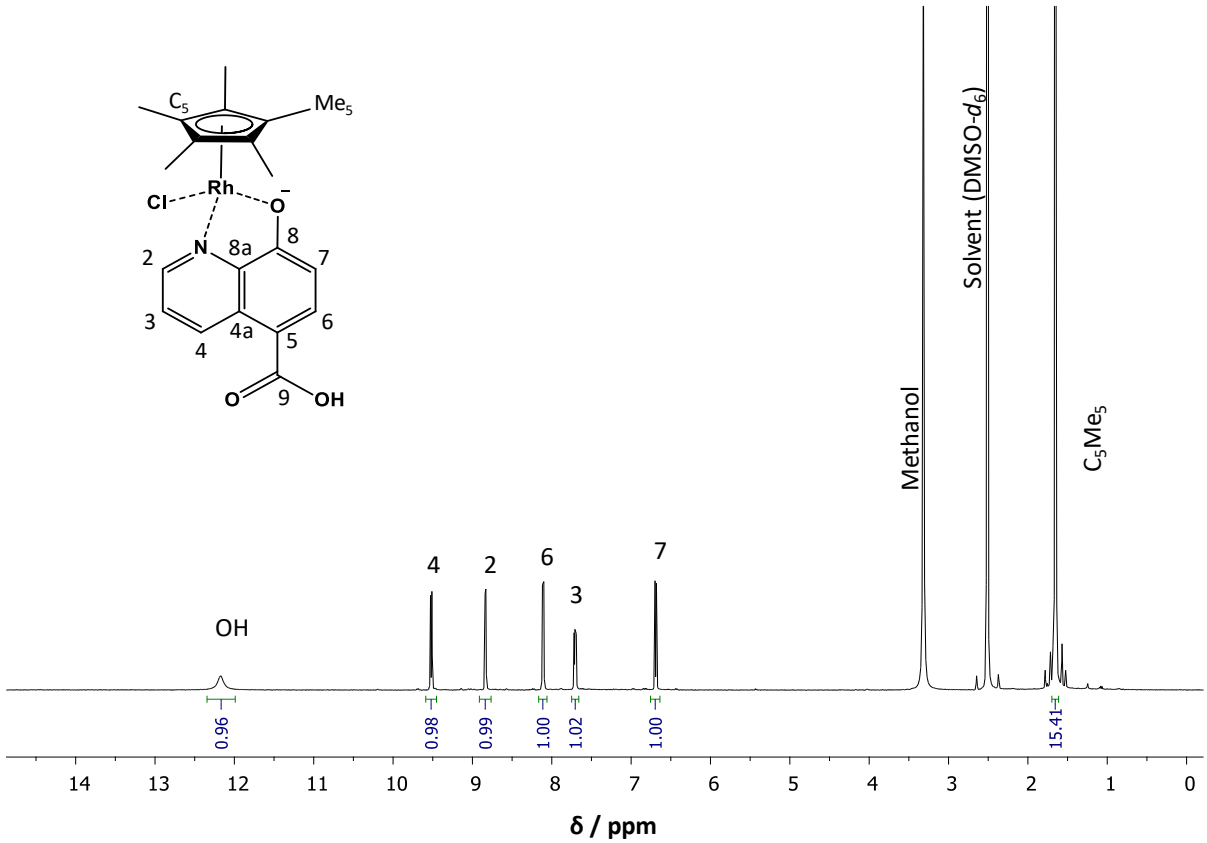

Figure S7. ^1H NMR spectrum of [RhCp*(LH)Cl] complex in DMSO-d_6. Numbering in the chemical structure corresponds to the labeled NMR peaks. {$c_{complex}$= 10 mM, T = 25.0 °C}

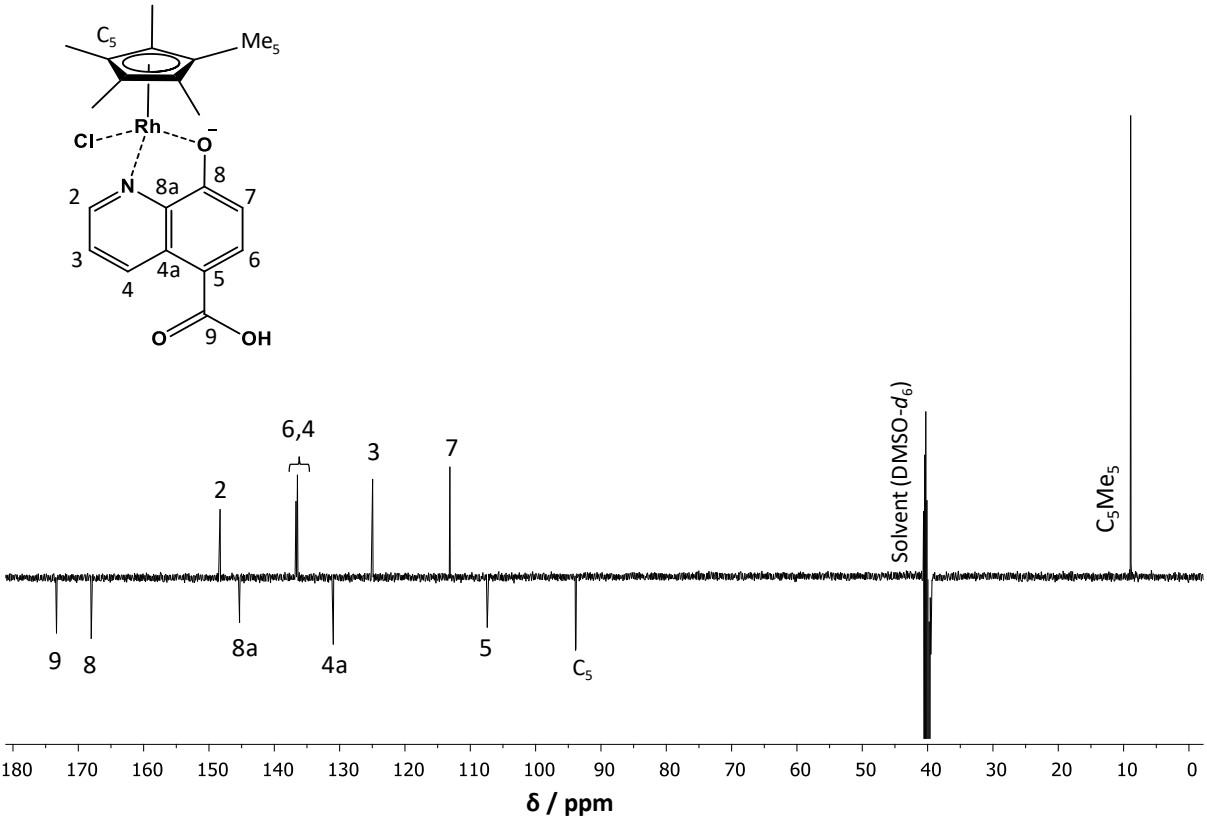

Figure S8. ^{13}C APT NMR spectrum of [RhCp*(LH)Cl] complex in DMSO-d_6. Attached proton test method: CH and CH_3 peaks are positive, C and CH_2 peaks are negative. Numbering in the chemical structure corresponds to the labeled NMR peaks. {$c_{complex}$ = 10 mM, T = 25.0 °C}

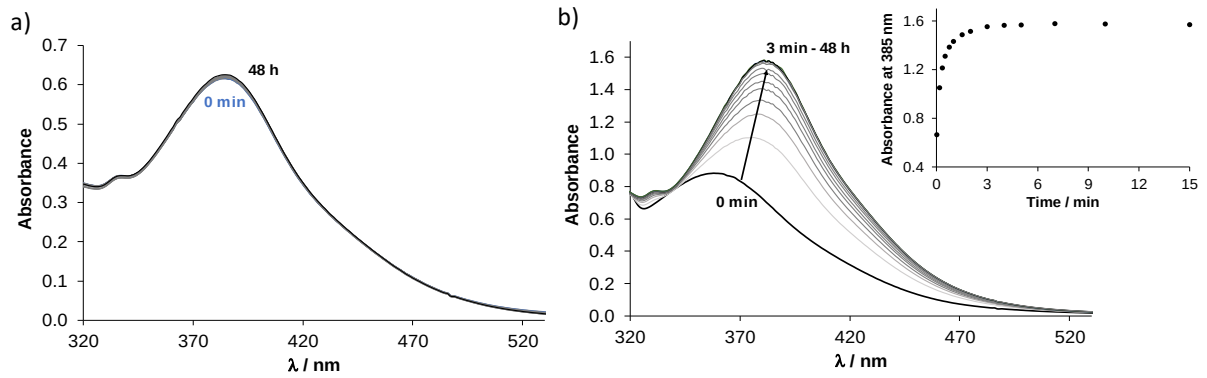

Figure S9. (a) UV-vis spectra of the isolated [RhCp*(LH)Cl] complex dissolved in PBS' at pH 7.4 recorded after 1 min (blue solid lines) and after 48 h (black solid lines), and (b) UV-vis spectra of $[RhCp^*(H_2O)_3]^{2+}$ – IOX1 (1:1) chemical system at pH 2.00 (0.01M KNO_3) at different time point. {(a) $c_{complex}$= 100 µM; (b) c_{RhCp^*} = c_{IOX1}= 200 µM; I = 0.2 M (KNO_3); ℓ = 1 cm; T = 25.0 °C}

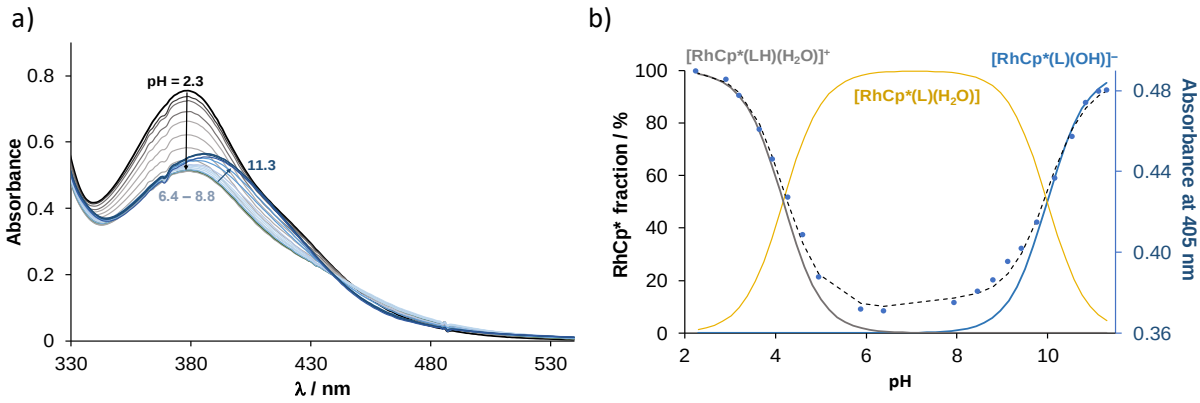

Figure S10. (a) UV-vis absorption spectra recorded for the $[RhCp^*(H_2O)_3]^{2+}$ – IOX1 (1:1) chemical system in the pH range 2.3 – 11.3. (b) Concentration distribution curves calculated for the same system based on the obtained pK_a values, and absorbance values at 405 nm at various pH values with the fitted curve (dashed line). {c_{RhCp^*} = c_{IOX1}= 80 µM; ℓ = 1 cm; I = 0.2 M (KNO_3); T = 25.0 °C}

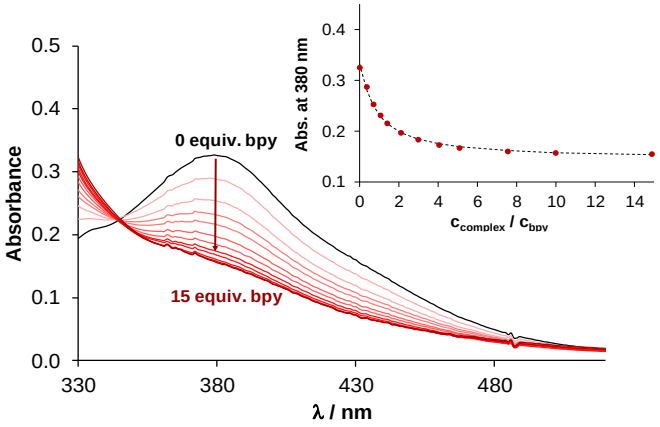

Figure S11. UV-vis spectra of RhCp* – IOX1 – bpy system at various bpy-to-complex ratios, and the inserted figure shows the absorbance values at 380 nm at various ratios with the fitted curve (dashed line). {c_{RhCp^*} = c_{IOX1}= 50 µM; c_{bpy} = 0 – 745 µM; ℓ = 1 cm; pH = 7.4 (20 mM phosphate buffer); I = 0.2 M (KNO_3); T = 25.0 °C}

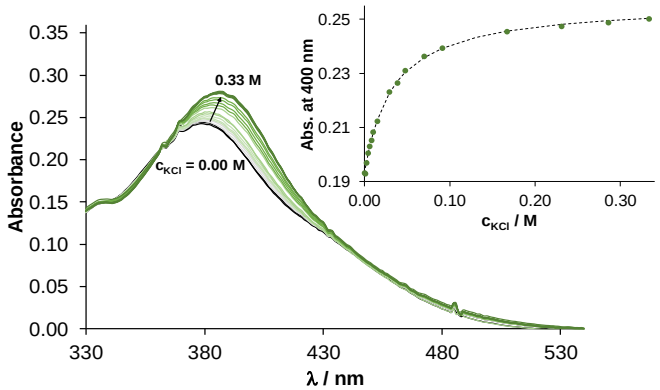

Figure S12. UV-vis spectra of RhCp* – IOX1 complex at pH 7.40 measured at various chloride ion concentrations, and the inserted figure shows the absorbance values at 400 nm at various chloride ion concentrations with the fitted curve (dashed line). {$c_{complex}$ = 80 µM; c_{KCl} = 0 – 0.33 M; ℓ = 1 cm; pH = 7.4 (20 mm phosphate buffer); T = 25.0 °C}

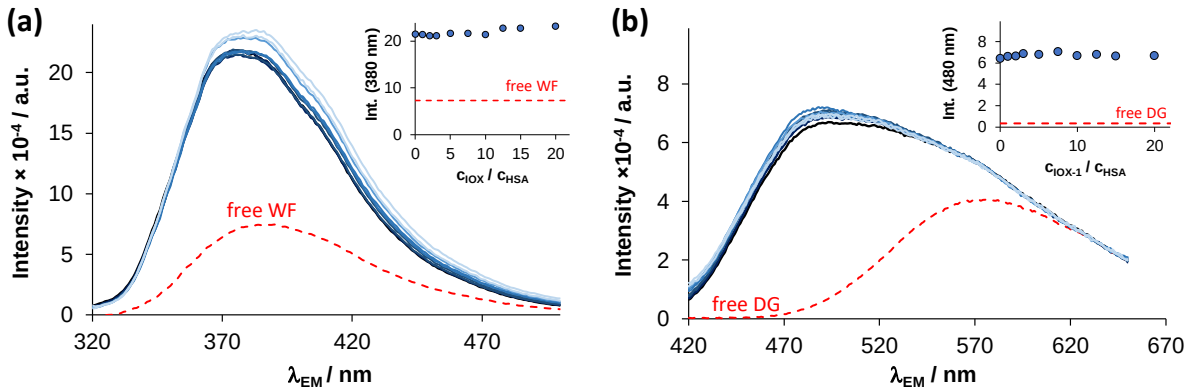

Figure S13. Fluorescence spectra recorded for the HSA – WF (a) and HSA – DG (b) systems in the presence of increasing IOX1 concentrations. The inserted figures show the intensities at the indicated λ_{EM} as a function of IOX1-to-HSA ratios. Dashed spectra denote the emission spectra of free site markers; IOX1 is non-fluorescent under the applied conditions. {$c_{HSA} = c_{site\ marker} = 1$ μM; $c_{IOX1} = 0$–20 μM; $\lambda_{EX} = 310$ nm (WF), 335 nm (DG); pH = 7.40 (PBS' with 2 mM EDTA); $T = 25$ °C}

Table S2. Initial composition of the samples prepared for equilibrium dialysis experiments, equilibrium concentrations, and free compound fractions obtained after the equilibrium was reached. UV-vis spectroscopy and Solver add-in of MS Excel were applied to determine free marker and IOX1 concentrations in the acceptor phase. {pH = 7.40 (PBS' with 2 mM EDTA), T = 25 °C}

	IOX1	HSA – IOX1	WF	HSA – WF	HSA – WF – IOX1	DG	HSA – DG	HSA – DG – IOX1
total concentrations in the donor phase prior to the dialysis (μM) V_{donor} **= 0.30 mL**								
c_{HSA}	0	103	0	103	103	0	103	103
c_{marker}	0	0	106	106	106	98	98	98
c_{IOX1}	202	202	0	0	202	0	0	202
concentrations after equilibration in the acceptor phase (μM) $V_{acceptor}$ **= 2.00 mL**								
[marker]$_{acceptor}$	-	-	13.6	6.8	7.9	13.1	8.2	9.2
[IOX1]$_{acceptor}$	25.2	20.1	-	-	20.5	-	-	21.8
concentrations after equilibration in the donor phase (μM) V_{donor} **= 0.30 mL**								
[marker]$_{donor}$	-	-	14.0*	6.8	7.9	13.9*	8.2	9.2
[HSA-bound marker]$_{donor}$	-	-	-	53.7	45.2	-	35.7	35.1
[IOX1]$_{donor}$	26.2*	20.1	-	-	20.5	-	-	21.8
[HSA-bound IOX1]$_{donor}$	-	46.4	-	-	44.4	-	-	34.8
free compound fraction (%) ([compound]$_{donor}$ / ([compound]$_{donor}$ +[HSA-bound compound]$_{donor}$))								
marker		-		11	15		19	21
IOX1		30		-	32		-	39

* Based on the UV-vis spectrum measured in the donor phase after equilibration.

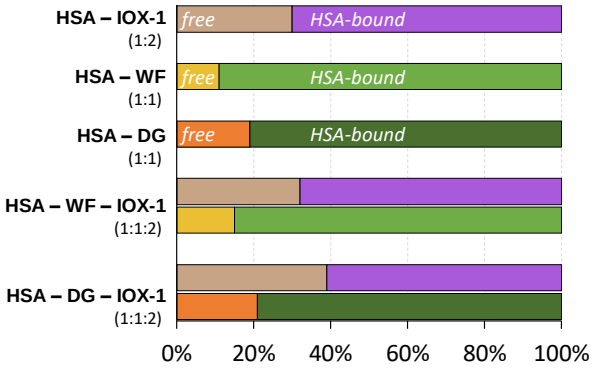

Figure S14. Free and protein-bound fractions of IOX1, WF, and DG in the indicated binary or ternary systems were determined in equilibrium dialysis assays. {c_{HSA} = 100 µM; V_{donor} = 0.300 mL, $V_{akceptor}$ = 2.00 mL; pH = 7.40 (PBS' with 2 mM EDTA); T = 25 °C}. *Note: the indicated concentration ratios apply to the initial sample composition, see details in Table S2*.

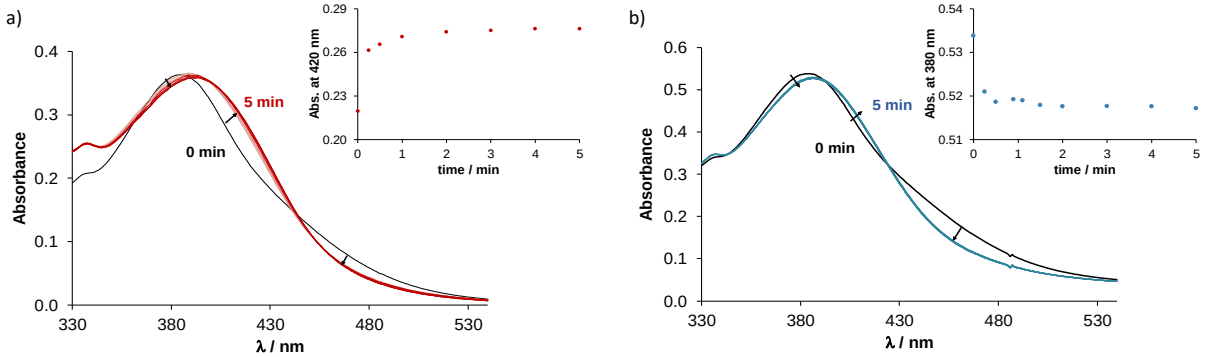

Figure S15. UV-vis spectra were recorded for RhCp* – IOX1 complex at pH 7.40 upon addition of (a) half equivalent of HSA and (b) one equivalent of MIM. Insert figures show the absorbance values at (a) 380 and (b) 420 nm plotted against time. {(a) $c_{complex}$ = 50 µM; c_{HSA} = 25 µM; (b) $c_{complex}$ = 75 µM; c_{MIM} = 75 µM; ℓ = 1 cm; pH = 7.40 (PBS'); T = 25.0 °C}

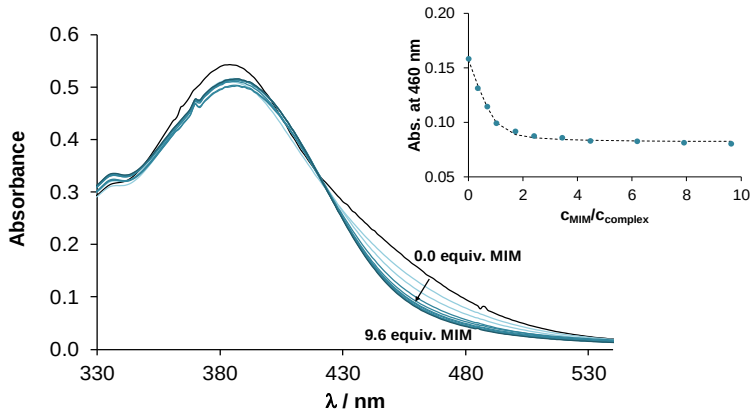

Figure S16. UV-vis spectra were recorded for the RhCp* complex of IOX1 upon addition of MIM at pH 7.4, and the inserted figure shows the absorbance change at 460 nm at various chloride ion concentrations with the fitted curve (dashed line). {$c_{complex}$ = 75 µM; c_{MIM} = 0 – 722 µM; ℓ = 1 cm; pH = 7.4 (PBS'); T = 25.0 °C}

Table S3. Primer crystallite size, hydrodynamic radius (R_h), polydispersity index (PDI), zeta potential, and IOX1 concentration of bare and IOX1-loaded LDH samples.

sample	primer crystallite size (nm)	R_h (nm)	PDI	Zeta potential (mV)	c_{IOX1} (mM)
LDH	24.8	38.6 ± 2.5	0.21 ± 0.01	32.3 ± 2.2	–
LDH/IOX1	10.8	58.4 ± 10	0.23 ± 0.02	26.5 ± 0.8	0.63 ± 0.01

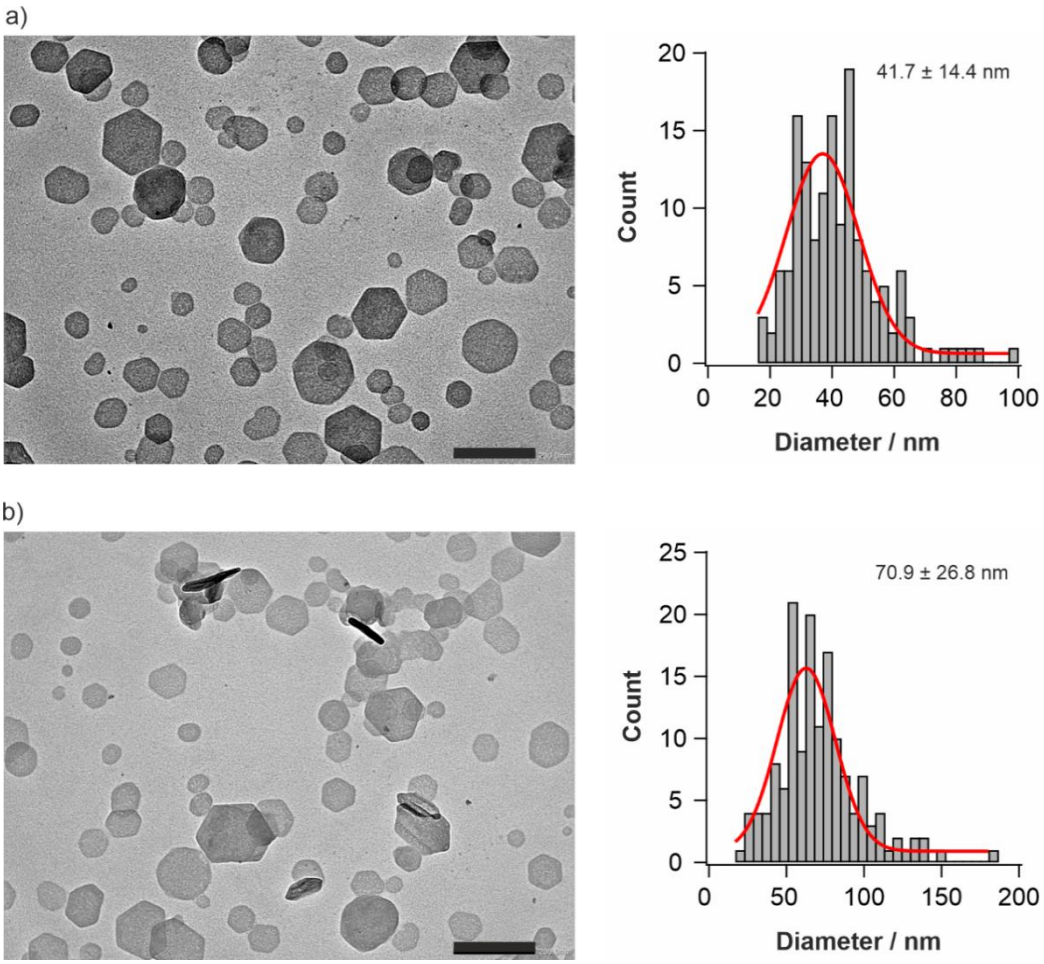

Figure S17. TEM micrographs and size distribution diagrams of (a) LDH and (b) LDH/IOX1. The average diameter with the standard deviation is indicated in the corner of each size distribution diagram. The scale bars represent 200 nm.

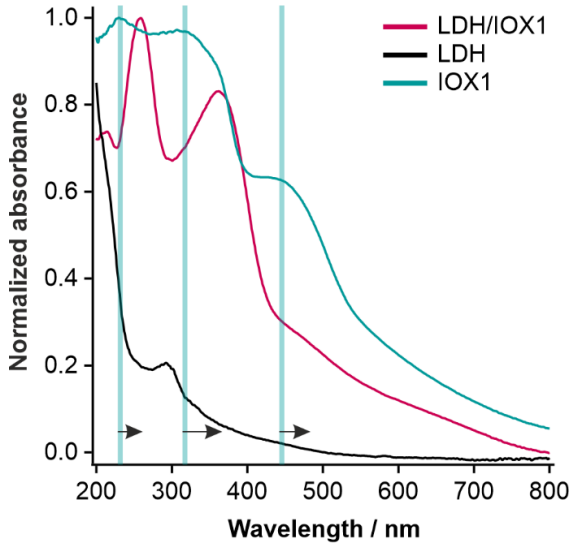

Figure S18. Solid-state UV-vis-diffuse reflectance (DRS) spectra of the LDH, IOX1, and LDH/IOX1 compounds.

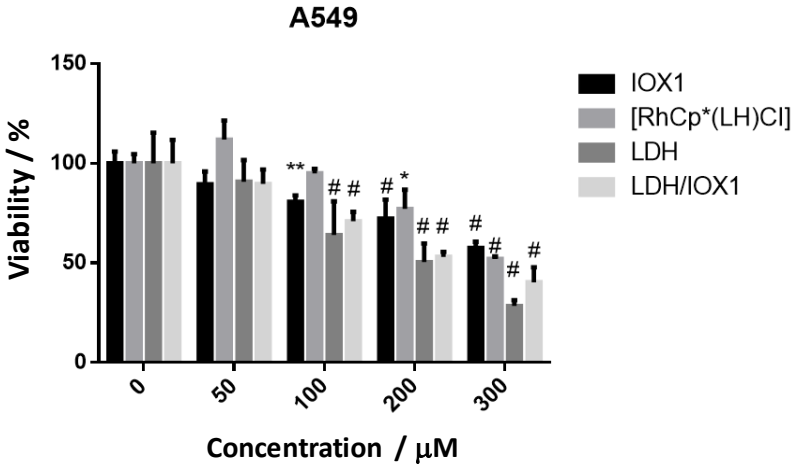

Figure S19. Viability of A549 cells upon IOX1, [RhCp*(LH)Cl], LDH, and LDH/IOX1 treatments. Two-way ANOVA, Dunnett's multiple comparisons test, *P < 0.05, **P < 0.01, #P < 0.0001.

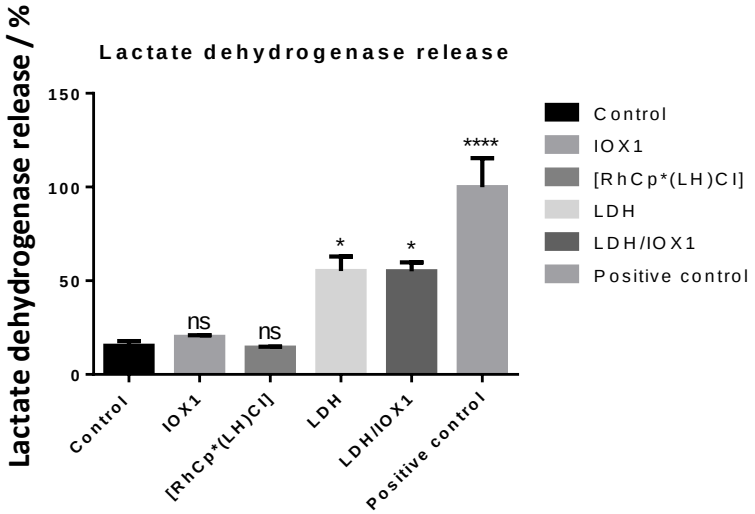

Figure S20. The cytotoxicity of IOX1, [RhCp*(LH)Cl], LDH, and LDH/IOX1 treatments on A549 cells was assessed by lactate dehydrogenase assay. One-way ANOVA, Dunnett's multiple comparisons test, *P < 0.05, ****P < 0.0001. Triton-X-100 was used as a positive control according to the manufacturer's instructions.

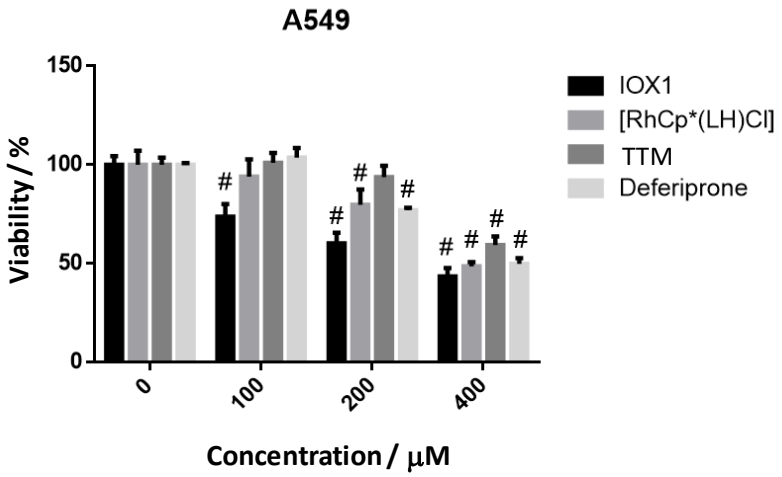

Figure S21. Viability of A549 cells upon individual IOX1, [RhCp*(LH)Cl], TTM, and deferiprone treatments. Two-way ANOVA, Dunnett's multiple comparisons test, $^{\#}P < 0.0001$.

Table S4. CI values calculated upon the IOX and TTM combinational treatments.

drug1	drug2	conc. (1) (µM)	conc. (2) (µM)	CI	inhibition (%)
IOX1	TTM	100	100	1.14	29
IOX1	TTM	200	100	1.07	45
IOX1	TTM	400	100	1.16	58
IOX1	TTM	100	200	1.44	29
IOX1	TTM	200	200	1.18	50
IOX1	TTM	400	200	1.19	64
IOX1	TTM	100	400	1.42	49
IOX1	TTM	200	400	1.51	57
IOX1	TTM	400	400	1.62	66

Table S5. CI values calculated upon the [RhCp*(LH)Cl] and TTM combinational treatments.

drug1	drug2	conc. (1) (µM)	conc. (2) (µM)	CI	inhibition (%)
[RhCp*(LH)Cl]	TTM	100	100	1.52	40
[RhCp*(LH)Cl]	TTM	200	100	1.44	16
[RhCp*(LH)Cl]	TTM	400	100	1.11	60
[RhCp*(LH)Cl]	TTM	100	200	1.34	12
[RhCp*(LH)Cl]	TTM	200	200	1.36	30
[RhCp*(LH)Cl]	TTM	400	200	1.38	59
[RhCp*(LH)Cl]	TTM	100	400	1.04	80
[RhCp*(LH)Cl]	TTM	200	400	1.12	84
[RhCp*(LH)Cl]	TTM	400	400	1.33	85

Table S6. CI values calculated upon the IOX1 and deferiprone combinational treatments.

drug1	drug2	conc. (1) (μM)	conc. (2) (μM)	CI	inhibition (%)
IOX1	deferiprone	100	100	0.70	45
IOX1	deferiprone	200	100	0.97	49
IOX1	deferiprone	400	100	1.08	61
IOX1	deferiprone	100	200	0.94	49
IOX1	deferiprone	200	200	1.16	53
IOX1	deferiprone	400	200	1.45	59
IOX1	deferiprone	100	400	1.37	61
IOX1	deferiprone	200	400	1.57	61
IOX1	deferiprone	400	400	1.51	75

Table S7. CI values calculated upon the [RhCp*(LH)Cl]and deferiprone combinational treatments.

drug1	drug2	conc. (1) (μM)	conc. (2) (μM)	CI	inhibition (%)
[RhCp*(LH)Cl]	deferiprone	100	100	0.67	33
[RhCp*(LH)Cl]	deferiprone	200	100	0.79	52
[RhCp*(LH)Cl]	deferiprone	400	100	0.99	69
[RhCp*(LH)Cl]	deferiprone	100	200	0.90	44
[RhCp*(LH)Cl]	deferiprone	200	200	1.05	56
[RhCp*(LH)Cl]	deferiprone	400	200	1.35	65
[RhCp*(LH)Cl]	deferiprone	100	400	1.43	55
[RhCp*(LH)Cl]	deferiprone	200	400	1.59	61
[RhCp*(LH)Cl]	deferiprone	400	400	1.78	73

Table S8. Collection of hydrolysis constants of Fe(III) and Fe(II). [a] {I = 0; T = 25 °C}

logβ	Fe(III)	Fe(II)
$[MH_{-1}]$	-2.2	-9.43
$[MH_{-2}]$	-5.71	-20.73
$[MH_{-3}]$	-12.26	-32.68
$[MH_{-4}]$	-21.6	–
$[M_2H_{-2}]$	-2.91	–

[a] Data taken from Ref. SI2.

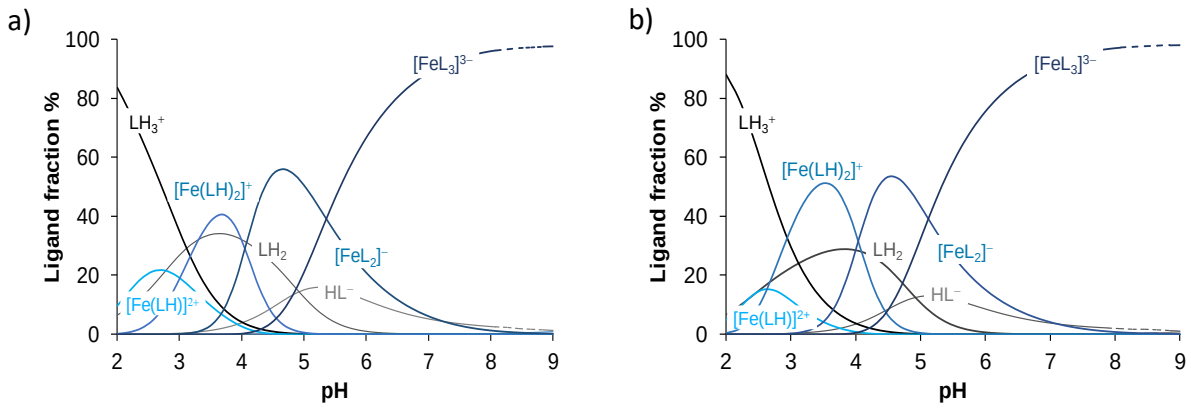

Figure S22. Concentration distribution curves calculated for Fe(III) – IOX1 (1:3) systems with hydrolysis constants for (a) I = 0.1 KNO_3 (($\log\beta$ for $[MH_{-1}]$ = –2.56, $[MH_{-2}]$ = –5.9, $[M_2H_{-2}]$ = –2.88) (b) I = 1.0 KCl ($\log\beta$ for $[MH_{-1}]$ = –3.21, $[MH_{-2}]$ = –6.73, $[M_2H_{-2}]$ = –4.09, $[M_3H_{-4}]$ = –7.58). Hydrolysis constants were taken from Ref. SI2. {c_{IOX1} = 161 µM, $c_{Fe(III)}$ = 53 µM}

Table S9. Conditions applied for steady-state spectrofluorometric measurements.

	c_{HSA} (µM)	c_{MARKER} (µM)	c_{IOX1} (µM)	λ_{EX} (nm)	λ_{EM} (nm)	slit widths EX/EM (nm/nm)
Trp214 quenching	1	–	0–60	295	310-500	4/4
WF displacement	1	1	0–20	310	320-500	4/4
DG displacement	1	1	0–20	335	420-600	5/5

CALCULATIONS APPLIED FOR THE EQUILIBRIUM DIALYSIS ASSAYS

Equilibrium dialysis assays were executed according to the following protocol: two parallel samples were always prepared.

Recovery of the compounds was determined by dialyzing samples containing the compounds only, and it is defined as follows:

$\{n_{\text{acceptor equilibrated}} + n_{\text{donor equilibrated}}\} / n_{\text{initial}}$;

where n = amount of substance. The equilibrium concentrations were determined by measuring the UV-vis absorbance spectrum in the acceptor and donor phases after equilibration and compared to that of the original (initial) sample. The recoveries of IOX1, WF, and DG are: 96%, 99% and 103%, respectively. Although 102% recovery is chemically meaningless, we did not correct the value to 100%. This error is a good indicator of the uncertainty of the method.

In the case of IOX1, it was also possible to determine the recovery of the compound directly in samples containing HSA, as the UV absorption of the compound is not sensitive to HSA binding, so it is sufficient to deconvolute the measured spectrum into the sum of the IOX1 and HSA spectra (see Figure S23a), the recovery of IOX1 in HSA – IOX1 samples was 98%.

Verifying the equilibration between the two compartments: according to the principle of equilibrium dialysis, the free compound (comp.) concentration must be the same in the acceptor and donor phases after equilibration ($[\text{comp.}]_{\text{acceptor}} = [\text{comp.}]_{\text{donor}}$). The validity of this condition was verified with samples containing the compounds only. Absorption spectra recorded for the donor and acceptor phases were nearly the same (Figure S23b)

Equilibrium concentrations listed in Table S2: In the binary systems, free compound concentration in the acceptor phase ([comp.]$_{acceptor}$) was determined on the basis of UV-vis absorption spectra, which is equal to [comp.]$_{donor}$. In ternary samples, the measured spectrum was deconvoluted to the sum of IOX1 and the site marker spectra (Figure S23c). HSA-bound compound concentrations are calculated as:

$$[comp.]_{donor} = (c_{total} \times V_{donor} - [comp.]_{donor} \times V_{donor} - [comp.]_{acceptor} \times V_{acceptor}) / V_{donor}$$

Free compound fractions: for this calculation, the equilibrium concentrations determined in the donor phase are considered only, since these concentrations express the strength of interaction with albumin. The formula used is shown in Table S2.

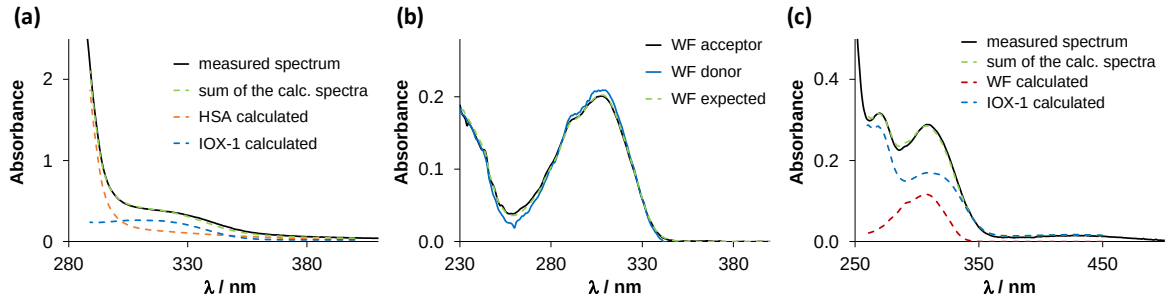

Figure S23. (a) Spectral deconvolution of a HSA – IOX1 donor phase sample UV-vis spectrum. (b) UV-vis spectra recorded in the donor and acceptor phases after equilibration of a WF sample; dashed spectrum denotes the "expected" spectrum when the original donor phase WF solution is distributed equivalently between both phases. (c) Spectral deconvolution of a HSA – WF – IOX1 acceptor phase sample spectrum into WF and IOX1 spectra.

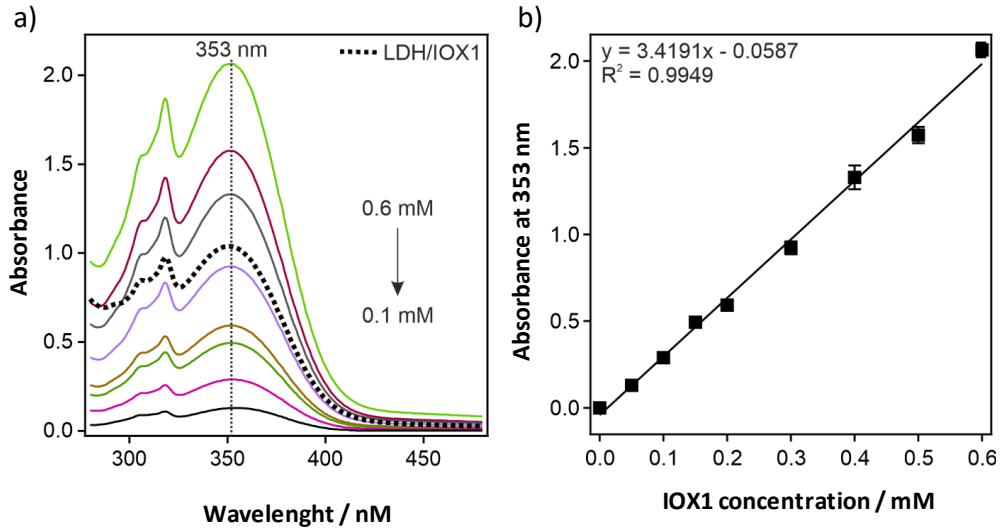

Figure S24. (a) UV-vis spectra of IOX1 in the 0.1 – 0.6 mM concentration range and LDH/IOX1 dissolved in HCl. (a) Calibration curve based on the absorbance values measured at 353 nm.

References

(SI1) J.T. Smith, V.M. Doctor, "Properties of binary complexes between metal ions and glyoxalic or alphaketoglutaric or imidazolypyruvic acid" *J. Inorg. Nucl. Chem.* **1975**, 37, 775.

(SI2) P. L. Brown, C. Ekberg, Hydrolysis of Metal Ions. Wiley, **2016**, pp. 135-145.